Steady-state numerical modeling of size effects in micron scale wire drawing

Juul, Kristian Jørgensen; Nielsen, Kim Lau; Niordson, Christian Frithiof

Published in:
Journal of Manufacturing Processes

Link to article, DOI:
10.1016/j.jmapro.2016.12.005

Publication date:
2017

Document Version
Peer reviewed version

Steady-State Numerical Modeling of Size Effects in Micron Scale Wire Drawing

K. J. Juul*, K. L. Nielsen, C. F. Niordson

Department of Mechanical Engineering, Solid Mechanics, Technical University of Denmark, DK-2800 Kgs. Lyngby, Denmark

Abstract

Wire drawing processes at the micron scale have received increased interest as micro wires are increasingly required in electrical components. It is well-established that size effects due to large strain gradient effects play an important role at this scale and the present study aims to quantify these effects for the wire drawing process. Focus will be on investigating the impact of size effects on the most favourable tool geometry (in terms of minimizing the drawing force) for various conditions between the wire/tool interface. The numerical analysis is based on a steady-state framework that enables convergence without dealing with the transient regime, but still fully accounts for the history dependence as-well as the elastic unloading. Thus, it forms the basis for a comprehensive parameter study. During the deformation process in wire drawing, large plastic strain gradients evolve in the contact region. This creates a need for a higher order plasticity theory to accurately predict the material behaviour across the multiple scales involved. The present study reveals that the contribution from an energetic (recoverable) length parameter is limited, while the corresponding dissipative contribution dominates and tends to shift the drawing force to a higher level. As a direct consequence, the strain gradient hardening effect reduces the most favourable tool angle of a sharp tool with up to 50 % (in terms of the required drawing force), whereas a circular shaped tool is proven less sensitive to scaling effects. By considering the contact force profile between tool and material it becomes clear that the strain gradients have a smoothing effect and both the mag-

*Corresponding author

Email address: krjoju@mek.dtu.dk (K. J. Juul)

nitude and position of the peak pressure are affected significantly. A round tool is found to reduce the peak force, while the location of the peak is found to move from outlet to inlet depending on the tool geometry.

Keywords: Steady-state, Size effects, Strain gradient plasticity, Metal forming, Wire drawing

1. Introduction

The wire drawing process is used in manufacturing at all scales, ranging from several centimetres to a few microns. The growing production of micro components has increased the demand for micro wires ($< 10\mu$m), which is an important component in e.g. semiconductors and electrical winding coils. At this scale, size effects are highly important in the production and therefore requires attention. It is well established that the size effect, appearing as either increased hardening or strengthening at the micron scale, originate from large strain gradients created by the inhomogeneous deformation during the wire drawing process.

Size effects can originate from two different sources, namely the effect of geometrically necessary dislocations (GNDs) which follows from the development of large plastic strain gradients and the effect of the microstructure when the grains become comparable in size to the wire diameter. The present study, however, investigates only the size effect related to the GNDs, while assuming homogeneity of the material, thus disregarding grain size effects. Storage of GNDs (Ashby, 1970; Gurtin, 2002; Ohno and Okumara, 2007) gives rise to free energy (energetic contribution) associated with the local stress field of the GNDs (dislocation pile-ups) and an increased dissipation (dissipative contribution) when the GNDs move through the lattice. The dissipative and energetic part are commonly referred to as length parameters in higher order plasticity theories. The length parameter ensures dimensional consistency in the model and essentially allows for a change in material behaviour across scales (see Mu et al. (2014) for a recent attempt to relate the length parameter to experimental findings at the micron scale). At the micron scale, GNDs can dominate the total dislocation density, which is normally dominated by statistically stored dislocations (SSDs) at larger scales. This leads to a requirement for additional energy to deform the material in the presence of large plastic strain gradients. This effect will create an apparent increase in yield stress as-well as additional hardening of the material.

To accommodate these issues, and develop a numerical model capable of handling this complex behaviour, the material model must represent the field quantities over the full range of length scales involved. In the present study, the higher order elastic-viscoplastic theory suggested by Fleck and Willis (2009) is employed. Here, the concept of higher order stresses, work-conjugate to the strain gradients, is adopted to increase the size range for which the material model is valid.

Neglecting grain and microstructure effects, the wire drawing process is a continuous process, making it ideal for a steady-state framework. Thus, the transient regime in the initial phase of the wire drawing process is not analysed in the present study. Avoiding the transient regime presents a number of advantages such as not having to deal with a continuously changing contact region (see e.g. Richelsen (1994) for a discussion related to a transient study of rolling). A numerical investigation of steady-state wire drawing at the micron scale can be found in Byon et al. (2009). Their work, however, is based on rigid plasticity where residual stresses and elastic unloading are neglected. At elevated temperatures (hot working), the effect of elastic unloading is minor, but at low temperatures (cold working), elastic unloading is essential. The steady-state model employed in the current study readily accounts for elastic unloading as-well as residual stresses, and it is based on the early work of Dean and Hutchinson (1980) for continuous crack growth (see also Wei and Hutchinson, 1997).

The developed model will be exploited to quantify the effect of strain gradients related to the most favourable tool geometry. During these studies both the effect of the dissipative and energetic length parameters are investigated (see e.g. Nielsen (2015) and Nielsen et al. (2016) for similar studies on steady-state rolling).

In the following sections, the basis for the model will be presented in tensor notation. The model is formulated in 2D, under the assumptions of axisymmetry, and thus the tensor notation should be interpreted as components 1,2,3 being the radial (r), axial (z), and angular (θ) direction, respectively. The notation $\dot{(\ )}$ is used for the time derivative of a quantity. This paper is divided into the following sections: The parametrization of the wire drawing process is presented in Section 2, the material model and the numerical formulation are presented in Section 3, the boundary value problem is presented in Section 4, results are presented in Section 5 and lastly concluding remarks are given in Section 6.

2. Parametrization of the Wire Drawing Process

The diameter of the undeformed wire is $2R_m$ and the reduced diameter after passing the tool is $2r_m$ (see Fig. 1). The tool consists of two linear parts (tool flanks) and a circular part (tool nose) of radius t_r. The linear and circular part of the tool is connected in the transition point, t_p, which is the point where the flank is tangent to the circle. For an increasing tool nose radius, t_r, the transitions points will move up, and ultimately they may coincide with the surface of the wire making the tool circular. The tool, as-well as the entire model, is revolved around the z-axis according to the axisymmetric formulation. Due to the axisymmetry, displacement constraints are not required along the z-axis, however symmetry conditions are enforced on the plastic strains such that $\dot{\varepsilon}^p_{12} = 0$ at $r = 0$. The tool is assumed to be rigid and the maximum reduction of the wire radius, Δ, is located at the centre of the tool ($z = 0$). The final radius of the wire, r_m, will then correspond to the initial radius, R_m, minus the reduction, plus an elastic spring back. The quantities, besides material parameters found in Tab. 1, which are prescribed in the model is the radial reduction ratio, Δ/R_m, the normalized tool nose radius, t_r/R_m, the tool angle, ϕ (also called the semi-cone angle), and the dimensionless inlet velocity, $\alpha = \dot{a}/(\dot{\varepsilon}_0 R_m)$, with $\dot{\varepsilon}_0$ being the material reference strain rate and $\dot{a}$ being the actual inlet velocity ($\alpha = 50$ throughout the study). The influence of the velocity is depending on the magnitude of the rate hardening of the material (exponent, m, in Eq. 5) and its influence can be significant.

3. Numerical Framework

The numerical framework builds on the gradient enhanced elastic-viscoplastic theory proposed by Gudmundson (2004); Gurtin and Anand (2005); Fleck and Willis (2009). Here, the analysis is restricted to small strains as a first approximation by limiting the wire reduction to a maximum of 4% (the overall straining in the wire drawing process is proportional to the wire reduction for small reductions). The total strain, ε_{ij}, is determined from the displacements, such that $\varepsilon_{ij} = (u_{i,j} + u_{j,i})/2$ which can be decomposed into an elastic part, ε^e_{ij}, and a plastic part ε^p_{ij} ($\varepsilon_{ij} = \varepsilon^e_{ij} + \varepsilon^p_{ij}$). The displacement and plastic strain components obey the principle of virtual work (PVW) presented in Eq. (1) (given in Cartesian components), and they are determined from the *Minimum Principles I and II* presented by Fleck and Willis (2009) (see also

Section 3.1).

$$\int_V (\sigma_{ij}\delta\varepsilon_{ij} + (q_{ij} - s_{ij})\delta\varepsilon^p_{ij} + \tau_{ijk}\delta\varepsilon^p_{ij,k})\mathrm{d}V = \int_S (T_i\delta u_i + M_{ij}\delta\varepsilon^p_{ij})\mathrm{d}S \qquad (1)$$

Here, q_{ij} is the micro-stress, σ_{ij} is the Cauchy stress, s_{ij} is the deviatoric stress, and τ_{ijk} is the higher order stress. The right-hand side of the PVW in Eq. (1) is divided into the conventional tractions $T_i = \sigma_{ij}n_j$ and the higher order tractions, $M_{ij} = \tau_{ijk}n_k$, where n_k is the unit outward normal vector to the surface S which bounds the volume V.

When including strain gradients in an axisymmetric model, essential non-trivial strain gradient components arise besides the trivial strain gradient components. The non-trivial out-of-plane strain gradient components are expressed in a local Cartesian frame as: $\varepsilon^p_{13,3} = \varepsilon^p_{31,3} = (\varepsilon^p_{11} - \varepsilon^p_{33})/r$, $\varepsilon^p_{23,3} = \varepsilon^p_{32,3} = \varepsilon^p_{12}/r$, where r is the radius at the point of evaluation (see e.g. Niordson, 2003).

According to the model proposed by Fleck and Willis (2009), the higher order stresses, τ_{ijk}, decompose into a dissipative part, τ^D_{ijk}, and an energetic part, τ^E_{ijk}, ($\tau_{ijk} = \tau^D_{ijk} + \tau^E_{ijk}$). The micro-stresses are assumed to have only a dissipative part i.e. $q_{ij} = q^D_{ij}$. The constitutive equations for the dissipative quantities read

$$q^D_{ij} = \frac{2}{3}\frac{\sigma_C[\dot{E}^p, E^p]}{\dot{E}^p}\dot{\varepsilon}^p_{ij}, \qquad \text{and} \qquad \tau^D_{ijk} = \frac{\sigma_C[\dot{E}^p, E^p]}{\dot{E}^p}L_D^2\dot{\varepsilon}^p_{ij,k} \qquad (2)$$

where σ_C is the gradient enhanced effective stress and $\dot{E}^p$ is the gradient enhanced effective plastic strain rate. In the present study, these take a quadratic from and read

$$\sigma_C = \sqrt{\frac{3}{2}q^D_{ij}q^D_{ij} + L_D^{-2}\tau^D_{ijk}\tau^D_{ijk}}, \qquad \text{and} \qquad \dot{E}^p = \sqrt{\frac{2}{3}\dot{\varepsilon}^p_{ij}\dot{\varepsilon}^p_{ij} + L_D^2\dot{\varepsilon}^p_{ij,k}\dot{\varepsilon}^p_{ij,k}} \qquad (3)$$

where L_D is the dissipative length parameter introduced for dimensional consistency.

In conventional plasticity, plastic dissipation is assumed to be related to the plastic deformations in terms of heat energy and cold work, while no free energy is associated with the plastic strains. However, in the presence of large plastic gradients (Ashby, 1970), the GND densities can become significant compared to the SSD densities. The GNDs give rise to the additional free energy associated with their local stress field. Thus, the total free energy is given by:

$$\Psi = \frac{1}{2}(\varepsilon_{ij} - \varepsilon^p_{ij})\mathscr{L}_{ijkl}(\varepsilon_{kl} - \varepsilon^p_{kl}) + \Psi_G \tag{4}$$

where Ψ_G accounts for the free energy associated with the GNDs. The conventional stresses are determined though the elastic relationship, $\sigma_{ij} = \partial\Psi/\partial\varepsilon^e_{ij} = \mathscr{L}_{ijkl}(\varepsilon_{kl} - \varepsilon^p_{kl})$, where $\mathscr{L}_{ijkl}$ is the isotropic elastic stiffness tensor and the higher order stresses are defined as $\tau^E_{ijk} = \partial\Psi/\partial\varepsilon^p_{ij,k}$. The free energy related to the GNDs is assumed to be quadratic with respect to the plastic strain gradients i.e. $\Psi_G = (GL^2_E\varepsilon^p_{ij,k}\varepsilon^p_{ij,k})/2$, and thus the higher order stresses are defined as $\tau^E_{ijk} = GL^2_E\varepsilon^p_{ij,k}$, where G is the elastic shear modulus and L_E is the energetic length parameter.

The current model is based on the power-law relation for the viscoplastic behaviour presented in Eq. (5).

$$\dot{E}^p = \dot{\varepsilon}_0 \left(\frac{\sigma_C}{g(E^p)}\right)^{1/m}, \qquad \text{with} \qquad g(E_p) = \sigma_y \left(1 + \frac{EE^p}{\sigma_y}\right)^N \tag{5}$$

Here, N is the strain hardening exponent, m is the strain rate hardening exponent, $\dot{\varepsilon}_0$ is the reference strain rate, and g is the flow potential. According to the viscoplastic model, the material will display significant viscous effects for large strain rate hardening exponents. On the contrary, for $m \to 0$, the material approaches a rate-independent response which corresponds to conventional J_2-flow plasticity in the limit where the dissipative and energetic length parameter is zero ($L_D \to 0, L_E \to 0$) (Nielsen and Niordson, 2014). It should be mentioned that this type of flow theory assumes the material to be isotropic at the micron scale and the model therefore omits any anisotropic evolution in the microstructure.

It should also be noticed, however, that the numerical framework becomes unstable for $L_D \to 0$. Hence, a conventional J_2-model without strain gradient effects has been developed separately for comparison in the limit case. The material parameters considered in the present study are collected in Tab. 1.

3.1. Steady-State Approach

A steady-state framework is chosen for the numerical analysis as it fits well with the nature of the wire drawing process. For a constant feed of material, and thus continuous deformation, a stationary field develops in the vicinity of the tool whereby the stress/strain fields remain unchanged to an observer fixed relative to the tool. Exploiting this in the modelling

makes the steady-state approach superior to the traditional transient Lagrangian models. Moreover, as the tool will remain stationary with respect to the computational finite element mesh one avoids numerical issues such as continuously changing contact interfaces. The steady-state finite element model employed in the present study is based on the early work by Dean and Hutchinson (1980), originally proposed for crack growth problems at a constant velocity. However, the technique can without modifications be adopted to a number of manufacturing processes such as e.g. wire drawing, rolling, welding etc. A key feature of the steady-state procedure by Dean and Hutchinson (1980) is that it implicitly accounts for elastic unloading for a wide range of constitutive models.

The steady-state condition states that any time derived quantity, $\dot{f}$, in a constitutive model can be related to the corresponding spatial derivative through the velocity, $\dot{a}$, along a streamline (illustrated in Fig. 1), according to the relation $\dot{f} = -\dot{a}\partial f/\partial z$. Thus, any incrementally defined quantity at a given material point can be evaluated by integrating along a streamline in the direction of the material movement, starting at a point upstream (z^0) of the tool and ending at the point of interest downstream (z^*). The point of interest (z^*) will then contain the history of all upstream points. The procedure for determining e.g. the plastic strains along the streamlines is shown in Eq. (6).

$$\varepsilon_{ij}^p(r^*, z^*) = \int_{z^0}^{z^*} \frac{\partial \varepsilon_{ij}^p}{\partial z} \mathrm{d}z, \qquad \text{with} \qquad \frac{\partial \varepsilon_{ij}^p}{\partial z} = -\frac{1}{\dot{a}} \dot{\varepsilon}_{ij}^p \tag{6}$$

The streamlines are defined as paths through neighbouring Gauss points on the same radius in the negative z-direction, making a mesh with only rectangular elements within the streamline domain ideal (see Fig. 1). The streamline integration is based on a forward Euler integration scheme where the time enters the calculations through the velocity, $\dot{a}$, in the steady-state framework.

In the adopted material model, the displacement field and plastic strain gradient rate field are determined separately following Fleck and Willis (2009). The displacement field is determined based on the conventional formulation for quasi-static problems shown in Eq. (7), corresponding to *Minimum Principle II* in Fleck and Willis (2009).

$$\int_V \mathscr{L}_{ijkl} \varepsilon_{kl} \delta \varepsilon_{ij} \mathrm{d}V = \int_S T_i \delta u_i \mathrm{d}S + \int_V \mathscr{L}_{ijkl} \varepsilon_{kl}^p \delta \varepsilon_{ij} \mathrm{d}V \tag{7}$$

The plastic strain gradient rate field is formulated as shown in Eq. (8)

corresponding to *Minimum Principle I* in Fleck and Willis (2009).

$$\int_V (q_{ij}^D \delta\dot{\varepsilon}_{ij}^p + \tau_{ijk}^D \delta\dot{\varepsilon}_{ij,k}^p)\mathrm{d}V = \int_V (s_{ij}\delta\dot{\varepsilon}_{ij}^p - \tau_{ijk}^E \delta\dot{\varepsilon}_{ij,k}^p)\mathrm{d}V + \int_S M_{ij}\delta\dot{\varepsilon}_{ij}^p \mathrm{d}S \quad (8)$$

The stationary solution is determined from the two minimum principles in a staggered iterative approach. Thus, each iteration in the process of obtaining a steady-state solution for the adopted gradient enhanced material model has two steps. The first step is to determine the displacements according to *Minimum principle II* (see Eq. (7)). From the displacements, the stress field is determined by taking the current straining history into account, and the obtained field is then feed into the second step. The second step is to determine the corresponding plastic strain rates, $\dot{\varepsilon}_{ij}^p$, according to *Minimum principle I* (see Eq. (8)). Employing a steady-state formulation, the plastic strain rates can be integrated along the streamlines in order to obtain the history dependent plastic strains, ε_{ij}^p. The conventional model corresponds to having both the length parameters equal to zero. In this case, *Minimum Principle I* is not required and a "conventional" viscoplastic relation can be employed to determine the plastic strains (see e.g. Nielsen and Niordson, 2012).

The implementation of the minimum principles follows the procedure suggested by Nielsen and Niordson (2014). According to this procedure, the displacement field discretization is based on a quadratic 8-node isoparametric element, and the plastic strain rate field discretization is based on a linear 4-node isoparametric element. Reduced Gauss integration is used for the displacement field (2x2 Gauss points), while full Gauss integration is used (2x2 Gauss points) for the plastic strain rate field. As an approximation, it is further assumed that the location of the Gauss points in the two element types are coinciding making the field quantities directly accessible for both parts of the solution scheme. The interaction between field quantities is based on the standard finite element interpolation shown in Eq. (9) for calculating quantities within the element at the points of evaluation.

$$u_i = \sum_{n=1}^{8} N^{(n)} u_i^{(n)}, \qquad \text{and} \qquad \dot{\varepsilon}_{ij}^p = \sum_{n=1}^{4} M^{(n)} \dot{\varepsilon}_{ij}^{p(n)} \quad (9)$$

For a more detailed overview of the algorithm see e.g. Nielsen et al. (2012).

4. Problem

Wire drawing under steady-state conditions is associated with large translational displacements, but the strains remain small for moderate reductions of the diameter. As an example; observe a point (r, z) located upstream at time zero in the model set-up illustrated in Fig. 1, and the same point (R, Z) at a later stage where it has moved downstream. The displacements, u_i, of this material point are then defined by the following relation:

$$Z = z - \dot{a}t + u_1 \qquad \text{and} \qquad R = r + u_2 \tag{10}$$

As the displacements, u_i, are relative to a frame translating with the inlet velocity of the wire, the total strains can be defined as $\varepsilon_{ij} = (u_{i,j} + u_{j,i})/2$.

In the first iteration on the displacement field, the tool geometry is introduced in the model as prescribed displacements in the radial direction. This ensures that the nodes are allowed only to slide along the rigid tool surface. Step one and two in the solution scheme creates a stress/strain field which is feed into the streamline integration handling the constitutive relations and history dependence which lead to an evolving plastic strain field. In the following iterations, the displacements and reactions forces are evaluated along the tool to determine whether a node should leave the tool (prescribed displacement condition removed) or if this particular node should have a prescribed displacement as it remains in contact with the tool.

In the contact region between the wire and the tool, friction forces are assumed to obey a Coulomb friction law. In the wire drawing process, the sliding direction will always result in a friction force in the positive z-direction (opposite direction of the material flow). The friction force is therefore purely kinematic, and can be determined as $F_f = \mu F_n$, where μ is the friction coefficient and F_n is the normal contact force. The friction force can thereby be determined from the reaction forces and be applied to the corresponding nodes. A force, corresponding to the sum of resisting forces acting on the nodes at the tool interface, is added to the left end of the wire. This sum of resisting forces corresponds to the required drawing force F_{draw}. In the current study, no restrictions on the higher order terms are applied in the contact region, i.e. no blocking of dislocations at the interface between the wire and tool has been introduced (the boundary is micro free and $\dot{\varepsilon}^p_{ij} \neq 0$).

5. Results

The gradient effects, related to the wire drawing process at the micron scale, are investigated in the following by exploiting the established numerical model. The results presented span over the effective plastic strains, the von Mises stresses, the effect of the friction coefficient, and the optimization of tool geometry.

In Figs. 2 and 3, the deformed shape, conventional effective plastic strain, $\varepsilon_e^p = [(2/3)\varepsilon_{ij}^p \varepsilon_{ij}^p]^{1/2}$, and von Mises stress, $\sigma_e = [(3/2)s_{ij}s_{ij}]^{1/2}$, are presented for two values of the dissipative length parameter. The plastic strains that develop during the wire drawing process are predicted to be rather inhomogeneous (see Figs. 2a and 3a). As the undeformed wire is drawn towards and through the tool, plastic straining rapidly evolves upon first contact. In fact, the plastic straining starts to evolve just in front of the tool as the material is forced toward the centre by the material further downstream closer to the tool. What is interesting to notice is that the drawn wire is leaving the tool with a rather inhomogeneous distribution of large plastic strains for a small dissipative length parameter (corresponding to a large scale of the wire drawing process), whereas a fairly homogeneous distribution is observed for a large dissipative length parameter (corresponding to a small scale of the wire drawing process). For wire drawing at large scales (Fig. 2), a concentration of large plastic strains is observed after the material has left the tool. The concentration is largest just below the surface and decreases towards the core of the wire. This is expected as the material from the surface region is flowing towards the core when the diameter is reduced. On the contrary, the magnitude of the plastic strains is a factor of 2 lower after the tool at the smallest scale (Fig. 3), while the plastic strains are of similar magnitude before the tool. This has to do with the increase in apparent yield stress typically found at the micron scale in regions with significant plastic strain gradients. Thus, plastic straining becomes less dominant which in turn gives rise to a larger elastic spring back. This is observed in Fig. 3 for a large dissipative length parameter, where it is seen that the material expands elastically after passing the tool center and continue to be in contact with the tool due to the increased spring back caused by the strengthening effect. The magnitude of the spring back corresponds to approximately 30% of the desired reduction in the smallest scale considered (Fig. 3). The results in Fig. 2 for small length parameter confirms this difference as the reduction after the tool corresponds approximately to the lowest point on the tool (actually the

radius is slightly smaller due to the elastic stretching of the material when the drawing force is applied).

An important consequence of the significant spring back, at small scales, is the necessity to compensate for the effect when designing the tool in order to achieve the desired diameter of the wire. In the present study, compensation for spring back has not been included in the model i.e. the wires in the different studies have different diameters after passing the tool. Hence, the forces are, in fact, expected to be even larger at a smaller scale than presented in the following, as a larger reduction would be required to obtain the desired diameter.

A comparison of the von Mises stress fields in Figs. 2b and 3b (presented as the normalized quantity, σ_e/σ_y) shows that the strengthening caused by the GNDs in the presence of large gradients leads to an increase in the stresses. It is seen that for both length parameters, residual stresses exist after passing the tool with the largest stresses near the surface. The stress state close to the surface can be of significance in relation to *stress corrosion cracking* depending on the material as not all materials are equally susceptible to this type of crack formation.

Figures 4 and 5 bring out the drawing force, F_{draw}, as it depends on the friction coefficient, μ, for two different tool geometries. In Fig. 4a, a sharp tool (small tool nose radius, t_r) is analysed for varying dissipative length parameter and reduction ratio. Observing the results for one of the curves in Fig. 4a, the required drawing force is increasing almost linearly with the friction coefficient. Moreover, when increasing the reduction ratio, the curves are simply shifting to a larger drawing force as the amount of deformation required is increasing (more energy needed). In addition to the shift, a slight increase in the slope is also observed. In a similar fashion, increasing the dissipative length parameter leads to an addition increase in the drawing force as the GNDs created by the gradients give rise to a strengthening effect as previously discussed (again, more energy is needed).

A similar analysis for the sharp tool, but with an energetic length parameter added to the material ($L_E/R_m = 0.1$), is presented in Fig. 4b. The energetic contribution reveals, however, only a very limited effect on the results. This has to do with the energetic contribution being linked to the free energy associated with the plastic strain gradients. At steady-state, a change in free energy is directly tied to the difference between the state of the material sufficiently far upstream and downstream from the tool. Thus, as the material upstream is assumed to have no prior history (zero gradients and

zero free energy stored), and combined with limited residual plastic strain gradients existing downstream, the free energy associated with the deformation process will be limited. This was also seen for the rolling process at small scales by Nielsen (2015). The energetic contribution is most evident for a small dissipative length parameter where it slightly increases the drawing force. However, the dissipative length parameter rapidly becomes dominant when increased.

Figure 5 presents a similar analysis but now for a tool with a much larger tool nose radius, t_r (referred to as a round tool). Comparing the results for the round tool (Fig. 5), with those for the sharp tool (Fig. 4), no significant differences are observed. Hence, the drawing force mostly depends on the material parameters and reduction ratio, and only little on the tool geometry.

To investigate the rather small effect of the tool geometry further, two additional studies have been conducted where the comparison of a sharp tool and a round tool is the main focus. The first part presented in Fig. 6 concerns optimization of the tool angle in order to minimize the drawing force for a sharp tool (small tool nose radius). In Fig. 6a ($L_E = 0$), the strengthening effect owing to strain gradients shifts the drawing force upward as the dissipative length parameter is increased (wire drawing at ever smaller scales). Moreover, it is evident that the most favourable tool angle, with respect to minimum drawing force, also changes. As indicated by enlarged circles in Fig. 6, an increase in the dissipative length parameter, decreases the most favourable tool angle (in agreement with the findings in Byon et al. (2009)). The impact on the most favourable tool angle is most significant for small dissipative length parameters, whereas the most favourable tool angle seems to stagnate for the larger dissipative length parameters. In fact, for sufficiently large dissipative length parameter ($L_D/R_m = 0.5$, see Fig. 6), the most favourable tool angle seems to start decreasing again (however, bear in mind the shallow nature of the minimum). Results for the conventional model, that ignores gradient effects, are also presented to illustrate that the gradient enhanced model converge towards the conventional limit for $L_E \to 0$ and $L_D \to 0$. The results are presented as the lower curve in Fig. 6a.

Conducting a similar investigation but now accounting for an energetic contribution (Fig. 6b), shows only a limited effect on the level of the drawing force when compared to the previous studies (compare Figs. 6a and 6b). However, the most favourable tool angle is somewhat more affected by including the energetic contribution, and as before the largest effect is observed for low dissipative length parameter. Moreover, the length scale effect

is again seen to stagnate for large dissipative length parameters.

The existence and decline of the most favourable tool angle for increasing length parameters in case of a sharp tool (demonstrated in Fig. 6) boils down to the competition between the evolution of plastic strain gradients and the friction in the contact region. For a low tool angle, the contact region is relatively long when compared to the region for larger angles. Thus, if the maximum reduction, Δ, remains the same this implies that the progressive change in the wire radius, as the material passes the tool, is lowest for a low tool angle. As the progressive change is lower, the plastic strain field will become more smooth i.e. smaller plastic strain gradients are expected. When the magnitude of the strain gradients decreases, the strengthening effect is also reduced, lowering the drawing force. Considering this as an isolated effect, the drawing force would continue to decrease as the angle decreases, however, at some point the drawing force starts to increase again. This is due to the presence of friction. For decreasing tool angles the length of the contact region increases, thus friction gradually becomes more dominant and leads to an increase in the drawing force. To confirm this competition of mechanisms, the analysis from Fig. 6a is repeated with a larger friction coefficient. As seen from Fig. 7, this shifts all the most favourable tool angles upward as friction becomes dominant at an earlier point.

A similar analysis is presented in Fig. 8 for a round tool ($t_r/R_m = 4.5$). Figure 8a indicates that the most favourable geometry remains at one specific tool angle regardless of the dissipative length parameter (with minor fluctuations). At this particular angle, the tool is not completely circular, but the flanks are very short so that the transition point is very close to the initial contact point. In fact, the material is only in contact with the circular part, as the material is forced down when approaching the tool before it interferes with the flanks. This is also seen from Fig. 8a as the drawing force becomes constant when increasing the tool angle because the material is only in contact with the circular part. The material is only in contact with the circular part for tool angles above 1.8°, making all solution to the right of this point identical. This also explains the fluctuations, as all the solutions on a horizontal line are identical with only the numerical convergence criteria to create a minor difference. From Fig. 8a, a circular tool seems to be the better shape in terms of the minimum drawing force across the scales for a zero energetic length parameter. However, with an energetic contribution (see Fig. 8b) the tool angle is observed to increase with the dissipative length parameter (largest impact for low dissipative length parameter). The tool

geometry, however, converges towards a shape where the material is only in contact with the circular part.

By changing the tool geometry, changes in the contact force profiles have been observed. Figure 9 displays four different geometries (top plot in each subplot) ranging from a sharp tool ($t_r/R_m = 0.25$) to a completely circular tool ($t_r/R_m = 7$). The corresponding contact force profile is presented below for an easy comparison, with $F_n^{(e)}$ being the normal force acting on an element in the contact zone and $A^{(e)}$ being the corresponding area of the element. Here, results are shown for different dissipative length parameters and zero energetic length parameter ($L_E = 0$). The transition from a sharp tool to a circular tool shows that the peak is moving from the outlet towards the inlet of the tool (most clearly seen for a small dissipative length parameter). The contact profile for the circular tool is similar to those reported by Richelsen (1991) and Nielsen (2015), where sheet rolling using a cylindrical roll is investigated. In addition, it is observed that the peak forces become smoother as the tool is rounded (t_r/R_m increases). For an increasing dissipative length parameter the peak contact forces increase, but the tendency remains the same. It is observed, however, that the peak becomes very wide and the shift from the inlet to outlet is less visible. This is a result of the increased strengthening associated with the strain gradients which tends to smear out the plastic strain field resulting in a wider peak.

What is interesting is the fact that the drawing force (area under the curves for a fixed length parameter) has approximately the same magnitude for the different geometries (also found in Figs. 4 and 5). In other words, as previously found, the energy associated with the wire drawing process is only affected slightly by the tool nose radius, t_r - with a slight reduction in drawing force as the tool is rounded (t_r increased). Thus, by choosing a particular tool shape, the peak pressure can be minimized without increasing the energy associated with the wire drawing process.

6. Concluding Remarks

The steady-state procedure by Dean and Hutchinson (1980) offers a straightforward approach to include history dependent elastic-plastic material behaviour into modelling the wire drawing process. Combined with the gradient enhanced elastic-viscoplastic material model by Fleck and Willis (2009), a basis for a comprehensive parameter study of size effects in wire drawing

at the micron scale has been established for small wire reductions. The key findings in the study are:

- Wire drawing at a small scale requires increased drawing force to accommodate the additional resistance due to the strengthening effect created by the geometrically necessary dislocations (GNDs). The dissipative length parameter is dominant in terms of forces involved in the drawing process, whereas the energetic length parameter only has a minor effect.

- As the friction coefficient is increased the required drawing force increases. Increasing the wire reduction ratio or the dissipative length parameter shifts the drawing force to a higher level. Comparing studies for a sharp and round tool (constant tool angle) showed no significant change in drawing force, indicating limited sensitivity to the tool nose radius, t_r.

- The most favourable tool angle is reduced significantly by gradient effects for a sharp tool (up to 50% depending on the parameters). The most rapid change in the most favourable tool angle is observed for small dissipative length parameters. As the dissipative length parameter increases, the most favourable tool angle tends to reach a constant value. The energetic length parameter primarily affects the studies with a small dissipative length parameter, reducing the most favourable angle further. By rounding the tool it was found that a circular shape (no flanks) is the most favourable across length scales (less sensitive to scaling effects).

- The contact force profile is affected significantly by the tool geometry. For a sharp tool, the peak pressure is located at the outlet, whereas for a circular tool the peak pressure shifts toward the inlet. For an increasing dissipative length parameter the contact forces increase. The gradient effect tends to have a smoothing effect on the contact force profile, by smearing out the peaks. For a fixed dissipative length parameter, the required drawing force is only affected little when changing the geometry. Choosing a smooth tool geometry can thereby reduce peak contact forces without increasing the drawing force.

During the entire study the reduction ratio, Δ/R_m, corresponds to the reduction at the centre of the tool. However, due to the spring back of the

material, the actual reduction of the wire will be smaller - in particular at the small scales where the strain gradient strengthening effect contribute to the elastic spring back.

7. Acknowledgement

The work is financially supported by The Danish Council for Independent Research in the project "New Advances in Steady-State Engineering Techniques", grant DFF-4184-00122.

References

Ashby, M., 1970. The deformation of plastically non-homogeneous alloys. Philos. Mag. 21, 399–424.

Byon, S. M., Moon, C. H., Lee, Y., 2009. Strain gradient plasticity based finite element analysis of ultra-fine wire drawing. J. Mech. Science & Technology 23, 3374–3384.

Dean, R. H., Hutchinson, J. W., 1980. Quasi-static steady crack growth in small-scale yielding. Fracture Mechanics: Twelfth Conference, ASTM STP700, American Society for Testing and Materials, 383–405.

Fleck, N. A., Willis, J. R., 2009. A mathematical basis for strain-gradient plasticity theory. Part II: Tensorial plastic multiplier. J. Mech. Phys. Solids 57, 1045–1057.

Gudmundson, P., 2004. A unified treatment of strain gradient plasticity. J. Mech. Phys. Solids 52, 1379–1406.

Gurtin, M., 2002. A gradient based theory of single-crystal viscoplasticity that accounts for geometrically necessary dislocations. J. Mech. Phys. Solids 50, 5–32.

Gurtin, M., Anand, L., 2005. A theory of strain-gradient plasticity for isotropic, plastically irrotational materials. J. Mech. Phys. Solids 53, 1624–1649.

Mu, Y., Hutchinson, J. W., Meng, W. J., 2014. Micro-pillar measurements of plasticity in confined cu thin films. Extreme Mech. Ltrs. 1, 62–69.

Nielsen, K. L., 2015. Rolling induced size effects in elastic-viscoplastic sheet metals. Euro. J. Mech. 53, 259–267.

Nielsen, K. L., Niordson, C. F., 2012. Rate sensitivity of mixed mode interface toughness of dissimilar metallic materials: Studied at steady state. Int. J. Solids. Struct. 49, 576–583.

Nielsen, K. L., Niordson, C. F., 2014. A numerical basis for strain-gradient plasticity theory: Rate-independent and rate-dependent formulations. J. Mech. Phys. Solids 63, 113–127.

Nielsen, K. L., Niordson, C. F., Hutchinson, J. W., 2012. Strain gradient effects on steady state crack growth in rate-sensitive materials. Eng. Frac. Mech. 96, 61–71.

Nielsen, K. L., Niordson, C. F., Hutchinson, J. W., 2016. Rolling at small scales. J. Manuf. Sci. Eng. 138, 041004.

Niordson, C. F., 2003. Strain gradient plasticity effects in whisker-reinforced metals. J. Mech. Phys. Solids 51, 1863–1883.

Ohno, N., Okumara, D., 2007. Higher-order stress and grain size effects due to self-energy of geometrically necessary dislocations. J. Mech. Phys. Solids 55, 1879–1898.

Richelsen, A.-B., 1991. Viscoplastic analysis of plane-strain rolling using different friction models. Int. J. Mech. Sci. 33, 761–774.

Richelsen, A.-B., 1994. Interface element modelling of friction in rolling. J. Mater. Processing Technology 42, 209–216.

Wei, Y., Hutchinson, J. W., 1997. Steady-state crack growth and work of fracture for solids characterized by strain gradient plasticity. J. Mech. Phys. Solids 45, 1253–1273.

List of Figures

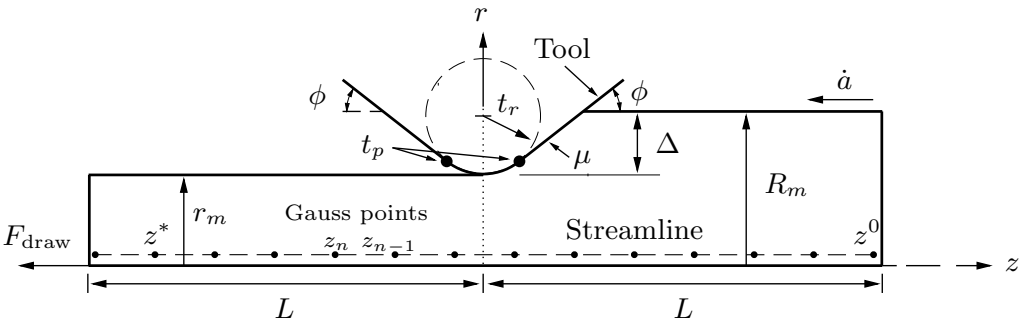

Figure 1: Parametrization of the wire drawing process in the adopted steady-state framework with axisymmetry around the z-axis. Throughout the study, $R_m/(2L) = 1/10$ and the finite element mesh employed consists of square elements with side length $L^{(e)}/R_m = 20$.

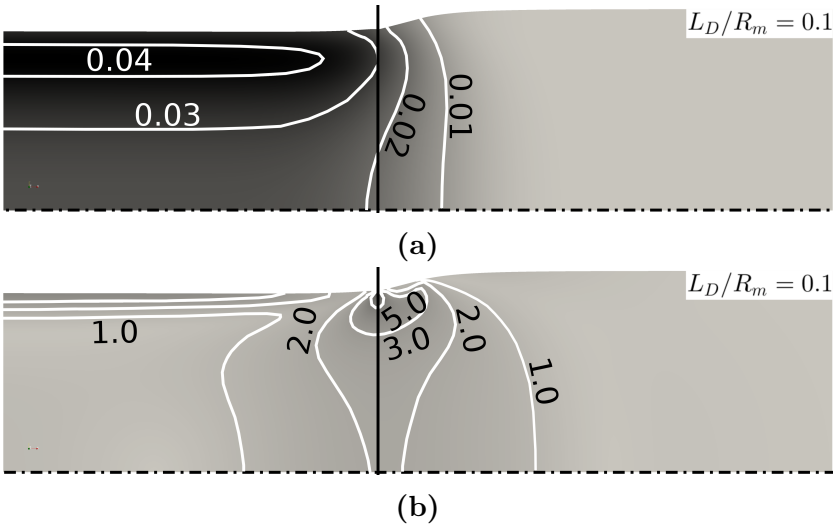

Figure 2: Effect of length parameter on field quantities (countour) and deformation (shape magnified by a factor of 10), where a) displays the effective plastic strain, ε_e^p, whereas b) shows the normalized von Mises stress, σ_e/σ_y. The solid black line indicates the tool center and the dash-dot line indicate the axis of symmetry. The dissipative length parameter and energetic length parameter remain fixed at $L_D/R_m = 0.1$ and $L_E = 0$, respectively ($\Delta/R_m = 0.01$, $\alpha = 50$, $t_r/R_m = 0.25$, $\mu = 0.1$, and $\phi = 1.5°$).

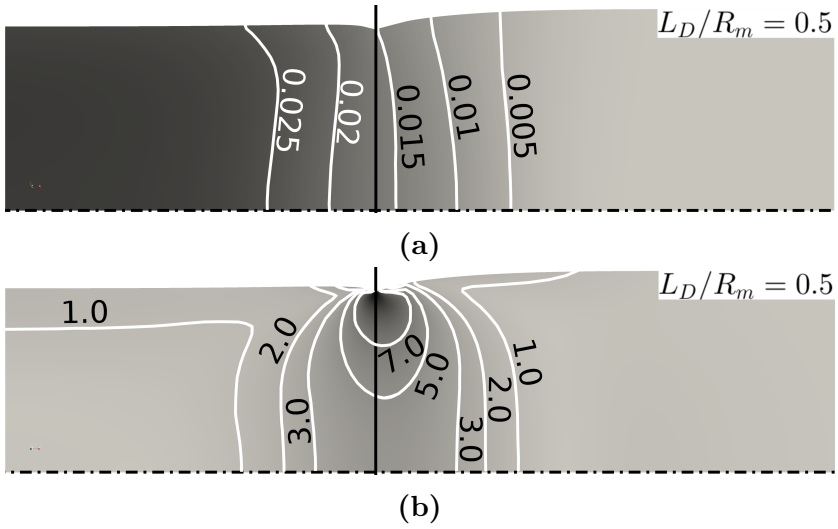

Figure 3: Effect of length parameter on field quantities (countour) and deformation (shape magnified by a factor of 10), where a) displays the effective plastic strain, ε_e^p, whereas b) shows away the normalized von Mises stress, σ_e/σ_y. The solid black line indicates the tool center and the dash-dot line indicate the axis of symmetry. For both models the dissipative length parameter and energetic length parameter remain fixed at $L_D/R_m = 0.5$ and $L_E = 0$, respectively ($\Delta/R_m = 0.01$, $\alpha = 50$, $t_r/R_m = 0.25$, $\mu = 0.1$, and $\phi = 1.5°$).

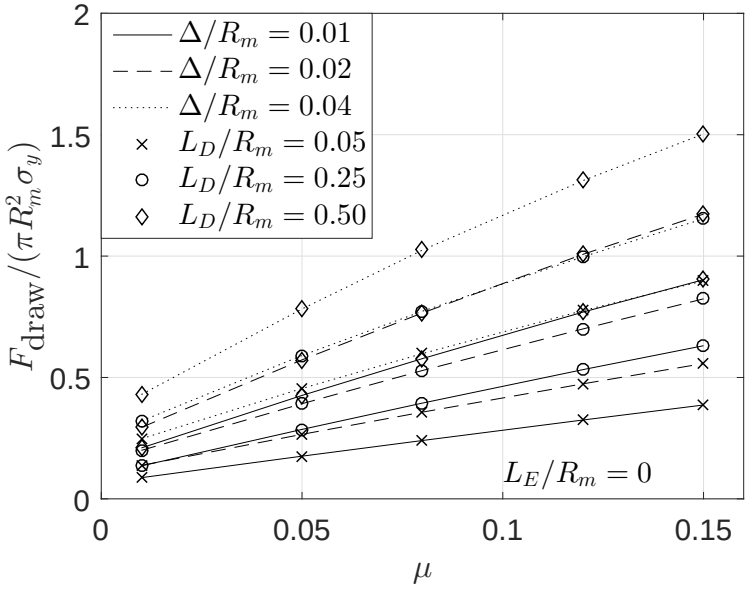

(a)

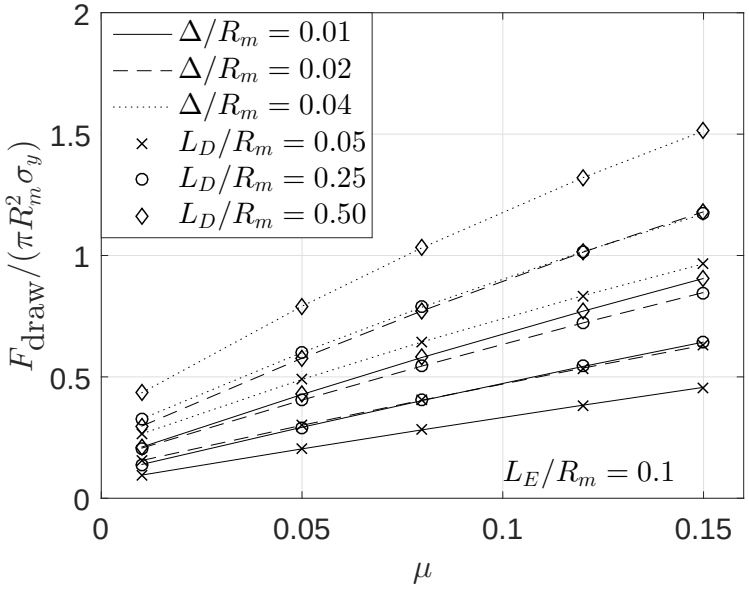

(b)

Figure 4: Required drawing force for a sharp tool ($t_r/R_m = 0.25$) as a function of the friction coefficient for various dissipative length parameters and wire reduction ratios. The velocity is fixed at $\alpha = 50$ and the tool angle is fixed at $\phi = 2°$. Here, shown for an energetic length parameter of a) $L_E/R_m = 0$, and b) $L_E/R_m = 0.1$.

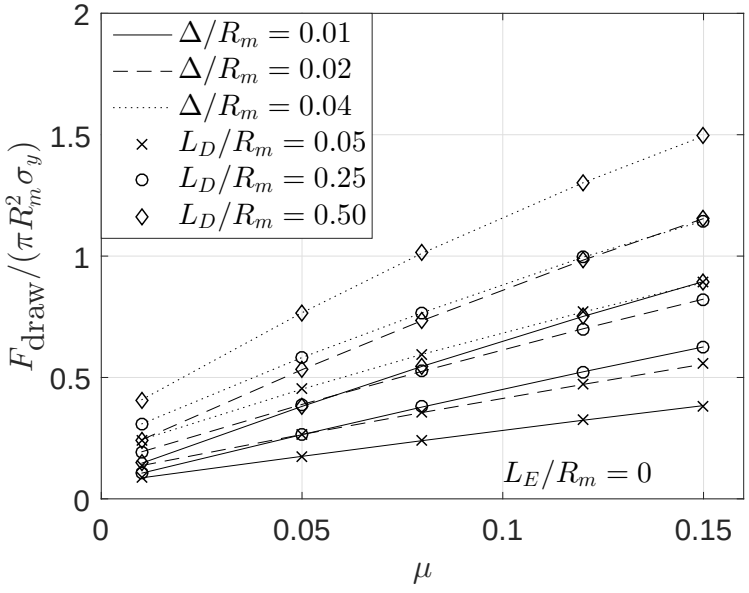

(a)

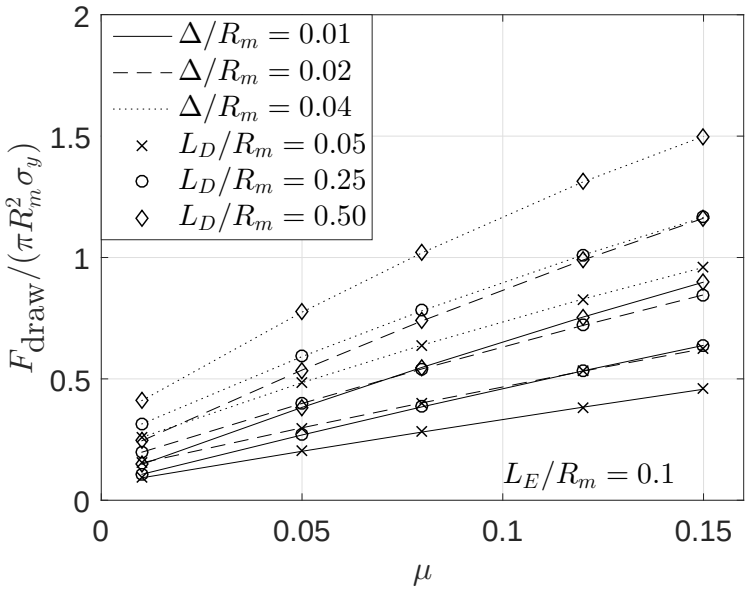

(b)

Figure 5: Required drawing force for a round tool ($t_r/R_m = 4.5$) as a function of the friction coefficient for various dissipative length parameters and reduction ratios. The velocity is fixed at $\alpha = 50$ and the tool angle is fixed at $\phi = 2°$. Here, shown for an energetic length parameter of a) $L_E/R_m = 0$, and b) $L_E/R_m = 0.1$.

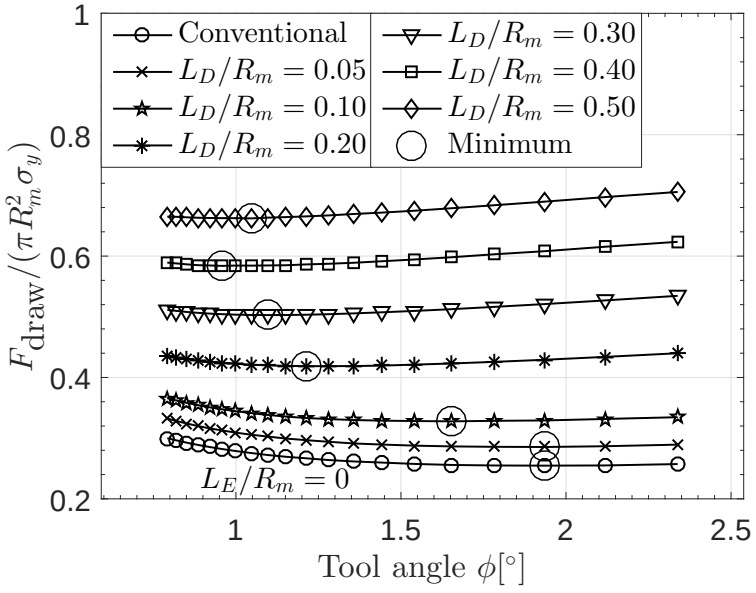

(a)

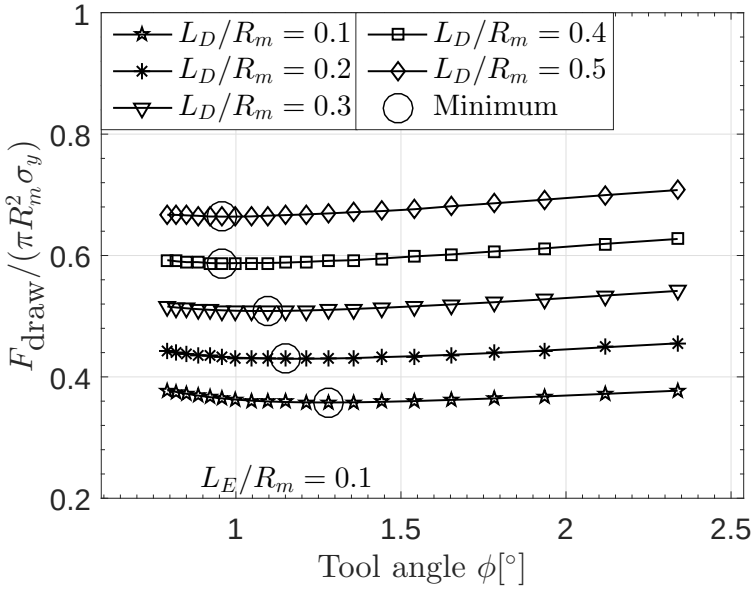

(b)

Figure 6: Required drawing force for a sharp tool ($t_r/R_m = 0.25$) as function of tool angle for different dissipative length parameters. The velocity is fixed at $\alpha = 50$, the reduction ratio at $\Delta/R_m = 0.01$, and the friction coefficient at $\mu = 0.1$. Here, shown for an energetic length parameter of a) $L_E/R_m = 0$, and b) $L_E/R_m = 0.1$.

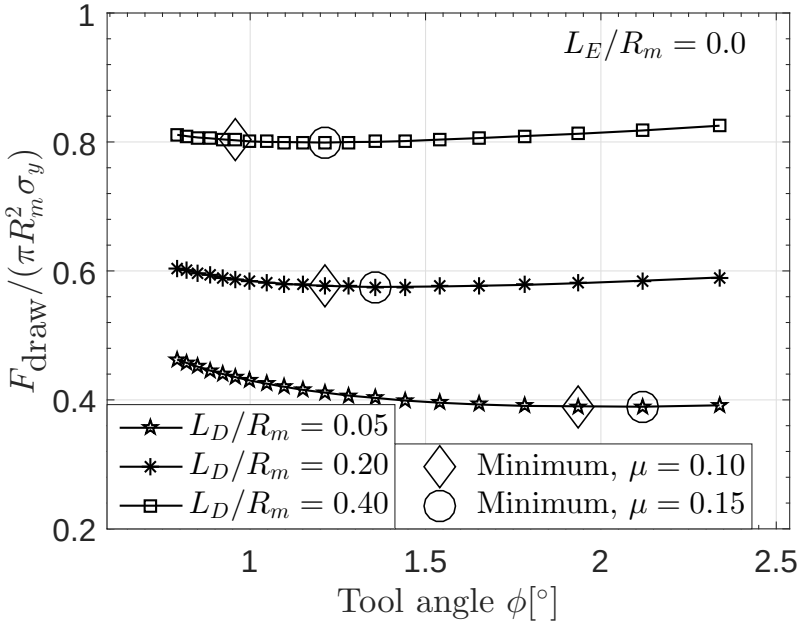

Figure 7: Required drawing force for a sharp tool ($t_r/R_m = 0.25$) as a function of the tool angle for different dissipative length parameters ($L_E/R_m = 0$). The velocity is fixed at $\alpha = 50$, the reduction ratio at $\Delta/R_m = 0.01$, and the friction coefficient at $\mu = 0.15$.

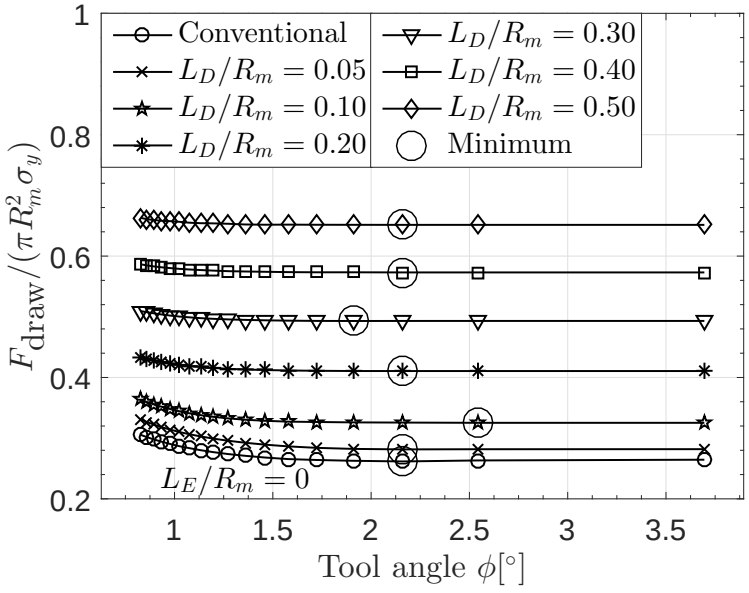

(a)

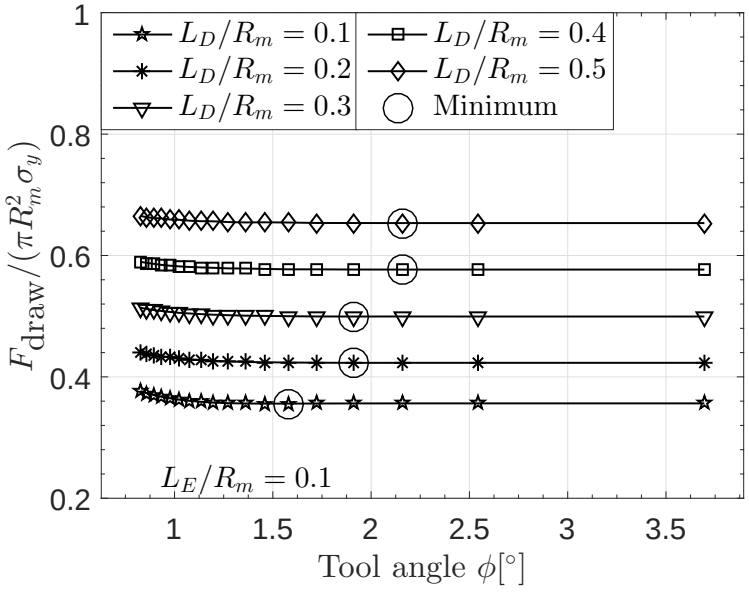

(b)

Figure 8: Required drawing force for a round tool ($t_r/R_m = 4.5$) as a function of the tool angle for different dissipative length parameters. The velocity is fixed at $\alpha = 50$, the reduction ratio at $\Delta/R_m = 0.01$, and the friction coefficient at $\mu = 0.1$. Here, results are shown for an energetic length parameter of a) $L_E/R_m = 0$, and b) $L_E/R_m = 0.1$.

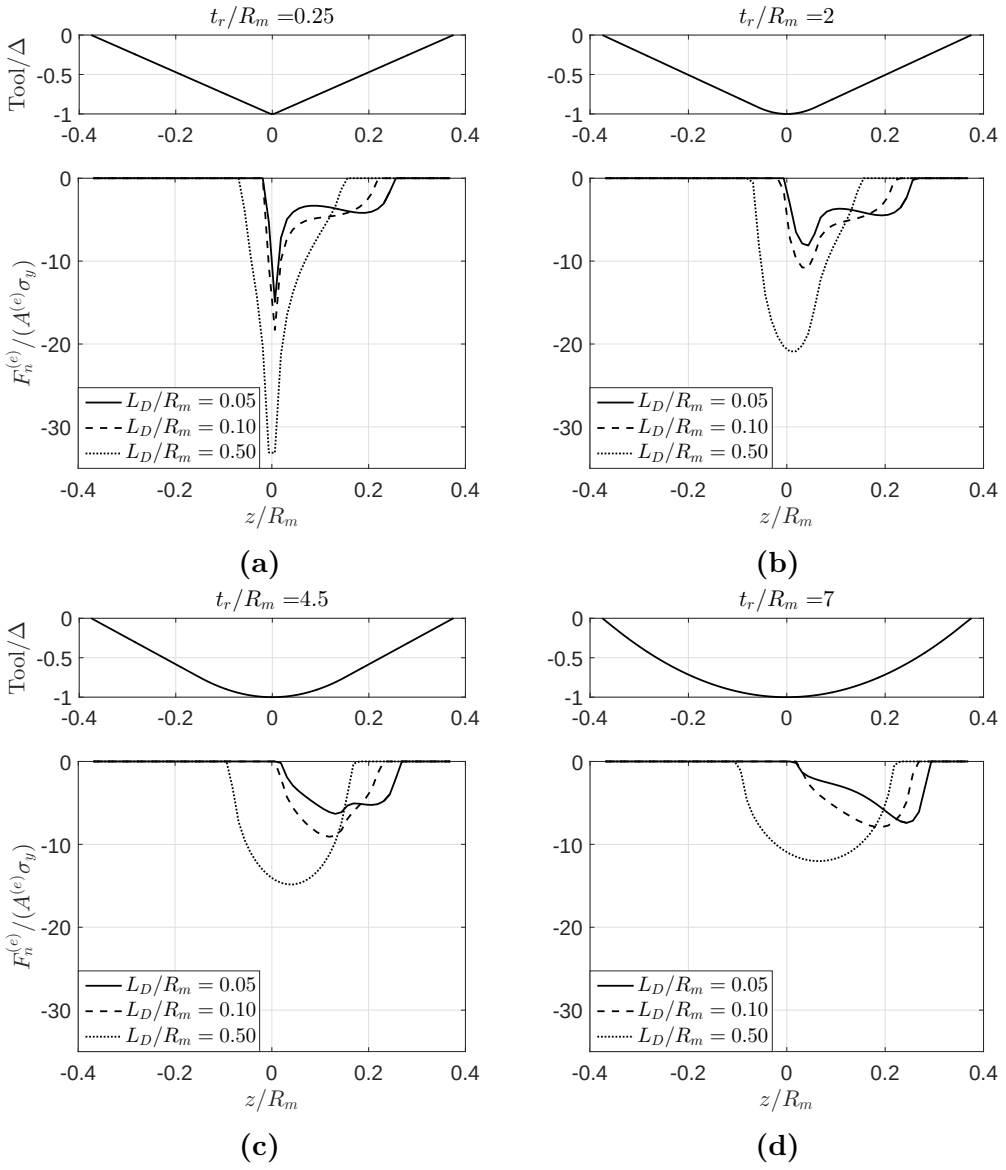

Figure 9: Contact forces (normal traction) at the interface between tool and wire for different dissipative length parameters ($L_E = 0$) and tool geometries. Subfigures (a),(b),(c),(d) each represents the tool geometry and corresponding contact force for different length parameters. The geometry $t_r/R_m = 0.25$ correspond to a sharp tool and $t_r/R_m = 7$ correspond to a completely circular tool. The velocity is fixed at $\alpha = 50$, the reduction ratio at $\Delta/R_m = 0.01$ and the friction coefficient at $\mu = 0.1$.

List of Tables

Parameter	Significance	Value
σ_y/E	Yield strain	0.001
ν	Poisson's ratio	0.3
N	Strain hardening exponent	0.2
m	Strain rate hardening exponent	0.02
$\dot{\varepsilon}_0$	Reference strain rate	0.001
L_D	Dissipative length parameter	0.05-0.5R_m
L_E	Energetic length parameter	0-0.1R_m

Table 1: Mechanical properties.